ISSN 2176-5480

22nd International Congress of Mechanical Engineering (COBEM 2013)
November 3-7, 2013, Ribeirão Preto, SP, Brazil

INFLUENCE OF UNIVERSAL JOINT ANGLES IN A LINEARIZED POWERTRAIN MODEL

Hugo Heidy Miyasato
Vinícius Gabriel Segala Simionatto
Milton Dias Junior
State University of Campinas, 200, Mendeleyev St, Barão Geraldo district, Campinas-SP, Brazil
hugomiyasato@gmail.com
vinicius.simionatto@gmail.com
milton@fem.unicamp.br

Abstract. *Theoretical models are used to predict and represent some Noise, Vibration and Harshness (NVH) phenomena of the automotive powertrain. This work intends to verify the influence of universal joint angles in a simplified rear wheel drive representation looking for changes on some important characteristics of the system, such as the shuffle and rattle modes calculated from linear models. The nonlinear equations of motion were linearized around equilibrium states for different combinations of universal joint angles and equilibrium positions. The Jacobian eigenvalues revealed unstable equilibrium and modal properties related to some powertrain phenomena.*

Keywords: *powertrain, universal joints, NVH, linearization, modal properties*

1. INTRODUCTION

An automotive powertrain or driveline is the system which transfers power from the engine to the wheels of the vehicle. Combustion engines based on the crank mechanism deliver output torques with great oscillations around its mean value, resulting in wide range of order content (Ligier and Baron, 2002). The whole torque delivery chain is built linking devices which may contain nonlinear characteristics. For example, the clutch may be represented by a stratified stiffness with energy dissipation due to friction and the transmission gear meshes may contain clearances that are represented by a dead-zone function (Couderc *et al.*, 1998).

As consequence of this complexity, some phenomena may occur only when all component are assembled together to work in operational conditions, what suggests that a system approach is imperative. Most of them are great concern in the Noise, Vibration and Harshness (NVH) field of study.

Some of these behaviors are observed through linear torsional models, once that the nonlinear response is not always excited significantly.

Shuffle is the response of a low frequency mode of the driveline found in range from 2 to 10 Hz according to [3]. It is excited when the driver executes a tip-in/tip-out excitation on the gas pedal. It is experienced as large or significant longitudinal vibrations of the vehicle. Drive rattle refers to a mode of operation where a high level of vibration occurs inside the transmission, usually between 40 and 80 Hz (Albers, 1994). Due to the clearances, the unloaded gear mesh pairs may generate impacts that are root cause of gear rattle noise.

"Cardan joints" or "Hooke's joints" are common denominations of universal joints (Schmelz *et al.*, 1992), couplings that allow torque transmission through misaligned shafts. They are widely used in rear wheel drive vehicles, trucks, buses, agricultural machinery, etc. Studies were conducted to study the influence of these joints on rotating machinery, once they generate secondary moments that cause the excitation of flexural vibrations in shafts (Ota and Kato (1984) and Browne and Palazzolo (2009)). Universal joint can cause also excite the shaft on its axial direction (Browne and Palazzolo, 2009). Few works relate these joints to automotive powertrain torsional system phenomena. Agricultural drivelines with these joints were studied by Crolla (1978) and Tiba (2006), who applied a much simpler function for the joint displacement restriction obtained by Duditza (1973).

In this work, a simplified rear wheel drive automotive powertrain model will be studied. First of all, equilibrium conditions for the double universal joint system will be determined. In a following step, the nonlinear equations obtained will be linearized and the Jacobian eigenvalues will be calculated for different combinations of joint angles and equilibrium states. Finally, the properties of these eigenvalues will be analyzed for stability and compared to characteristics found in the linear representation related to powertrain phenomena.

1.1 Universal joint approximate function

Figure . 1(a) shows a representation of a cardan joint, where the cross ABCD (shown in Fig. 1(b)) transmit an input torque T_{in} from one yoke to the other, namely T_{out}, located on two different planes, xy and x'y'. The joint angle β formed between axis z and z' indicates the misalignment between planes. Having this configuration in mind, Fig. 1(a) can

ISSN 2176-5480

be simplified to Fig. 1(b).

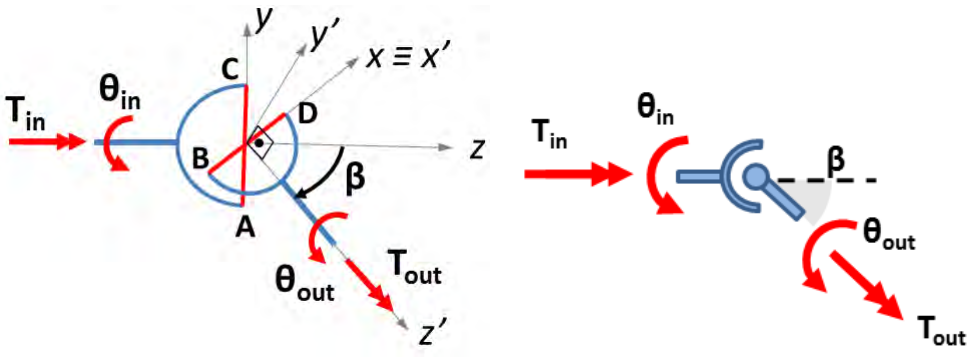

(a) (b)

Figure 1. Diagram representing a universal joint (a) and a simplified scheme with its main features (b).

Poncelet proved that relations between inputs (θ_{in} and $\dot{\theta}_{in}$) and outputs (θ_{out} and $\dot{\theta}_{out}$) in a single universal joint was not uniform (Schmelz *et al.*, 1992), reaching expressions for displacements (Eq. (1)) and speeds (Eq. (2)).

$$\tan\theta_{in} = \tan\theta_{out}\cos\beta \tag{1}$$

$$\frac{\dot{\theta}_{out}}{\dot{\theta}_{in}} = \frac{\cos\beta}{1-\sin^2\beta\cos^2\theta_{in}} \tag{2}$$

The universal joint may also transmit variable torque, once that power transmitted by a frictionless joint is constant (Ota and Kato, 1984), depending on the speed ratio of Eq. (2):

$$T_{out}\dot{\theta}_{out} = T_{in}\dot{\theta}_{in} \tag{3}$$

Tiba (2006) used approximate expressions obtained by Duditza (1973), instead of Eq. (1) and (2). Equation (4) clearly shows that the output angle of the joint results from the input angle with a fluctuation depending on the joint angle and the input angular position. The simplified speed ratio is calculated by a much simpler differentiation from the approximate (Eq. (5)).

$$\theta_{out} = \theta_{in} + \frac{\beta^2}{4}\sin(2\theta_{in}) \tag{4}$$

$$\frac{\dot{\theta}_{out}}{\dot{\theta}_{in}} = 1 + 2\frac{\beta^2}{4}\cos(2\theta_{in}) \tag{5}$$

Figure 2(a) makes a comparison between the computational representation of Eq. (1) and (4) for an input rotation angle between -180° and 180°. Original and approximate speed ratios are shown in Fig. 2(b):

In most of programming languages, such as C, Java™ and MATLAB® the arctangent function is defined only for angles between -90° and 90°. Handling values out of this range causes sudden changes of values as seen on the computational implementation of the original function (Eq. (1)) in Fig. 2(a). This behavior may lead to the introduction of undesirable harmonics to a simulation with no consistent physical meaning. Figure 3(a) shows a maximum output angle error is found below 0.2 % between the original and approximate expressions with $\beta = 20°$. The speed ratio error is very small, reaching maximum error below 0.004 % as presented in Fig. 3(b).

2. NONLINEAR POWERTRAIN FORMULATION

The rear wheel drive model is shown in Fig. 4(a). The flywheel, with angular displacement θ_F, is connected to the transmission through the clutch stiffness, inserted as a linear spring element k_C. Coordinates θ_{Tin}, θ_{Sec} and θ_{Tout}, are used to describe the input, secondary and output shafts, respectively. Gear pitch radiuses are represented by r_i. The total

ISSN 2176-5480

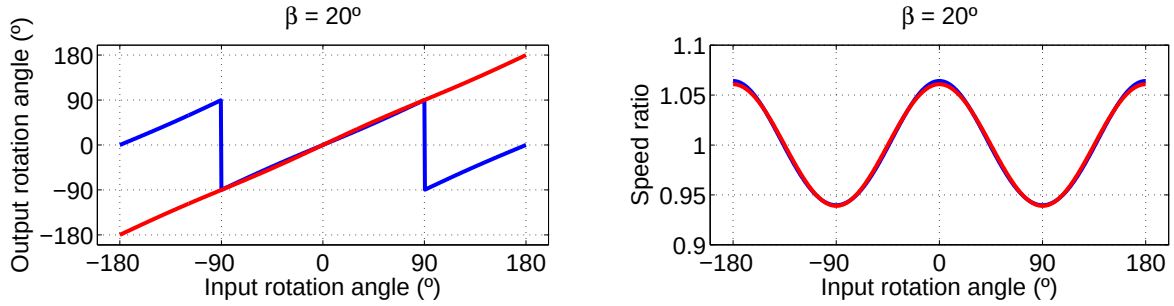

(a) (b)

Figure 2. Computational implementation of the original functions ( ) and their approximations ( ) compared in terms of angular position (a) and speed ratio (b).

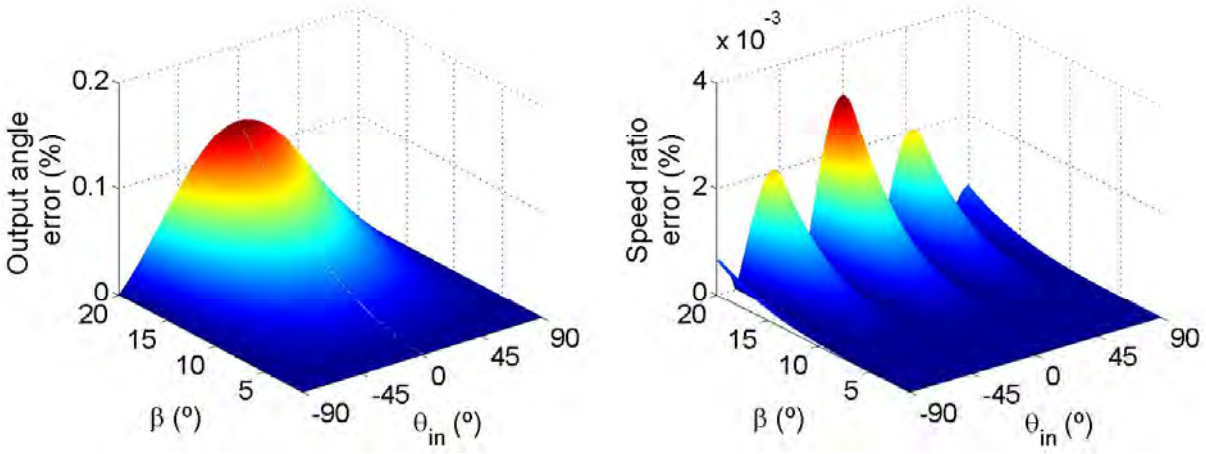

(a) (b)

Figure 3. Diagram representing a universal joint (a) and a simplified scheme with its main features (b).

transmission gear ratio is $n_T = n_{T1}n_{T2}$, with $n_{T1} = r_2/r_1$ and $n_{T2} = r_4/r_3$. Joints H_i have misalignment angles β_i and output angles θ_{Hi}. They are arranged in a Z-configuration with in-phase yokes, which avoid non-uniformity in speed transmission for parallel rigid shafts when $\beta_1 = \beta_2$ [4]. Final drive ratio at the differential is calculated by $n_D = r_6/r_5$. Angles θ_{Din} n and θ_{Dout} represent the differential input and output, while θ_W refers to the wheels. The driveshaft and the side shaft's stiffness are called k_D and k_W, respectively. All inertial elements are marked as I_i. The linear model is derived adopting $\beta_1 = \beta_2 = 0°$ (Fig. 4(b)).

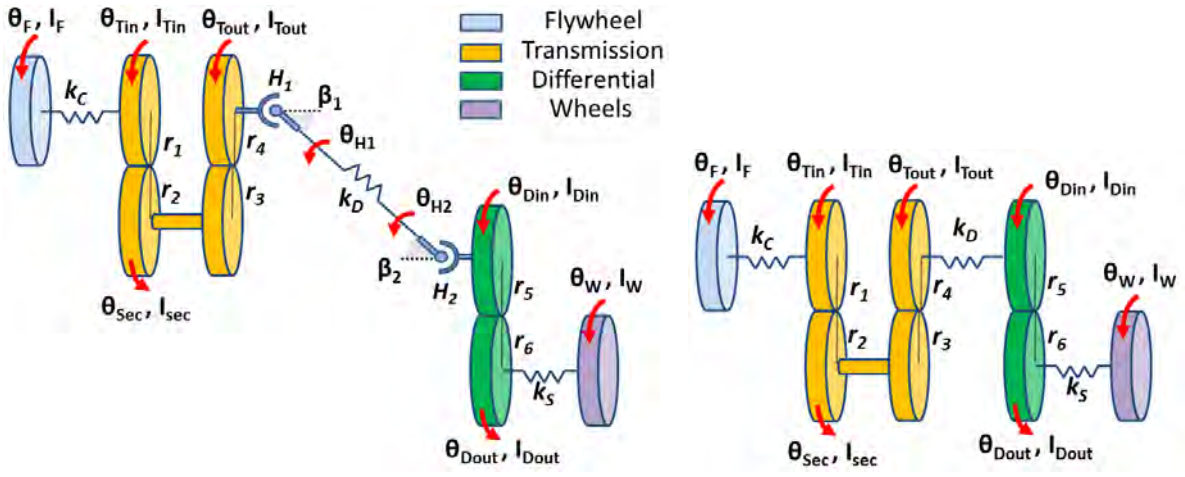

(a) (b)

Figure 4. Powertrain model with cardan joints H_1 and H_2 in Z configuration (a) and its linear representation (b).

Joint displacement restrictions are shown in Eq. (6) and (7). The oscillatory components are represented by functions

ISSN 2176-5480

$g_1(\beta_1, \theta_{Tout})$ and $g_2(\beta_2, \theta_{Din})$:

$$\theta_{H1} = \theta_{Tout} + g_1(\beta_1, \theta_{Tout}) \tag{6}$$

$$\theta_{H2} = \theta_{Din} + g_2(\beta_2, \theta_{Din}) \tag{7}$$

Speed ratios are represented by functions $f_{H1}(\beta_1, \theta_{Tout})$ and $f_{H2}(\beta_2, \theta_{Din})$:

$$\frac{\dot{\theta}_{H1}}{\dot{\theta}_{Tout}} = f_{H1}(\beta_1, \theta_{Tout}) \tag{8}$$

$$\frac{\dot{\theta}_{H2}}{\dot{\theta}_{Din}} = f_{H2}(\beta_2, \theta_{Din}) \tag{9}$$

The state space can be represented by the following coordinates:

$$\{y\} = \left\{ \begin{array}{cccccccc} y_1 & y_2 & y_3 & y_4 & y_5 & y_6 & y_7 & y_8 \end{array} \right\}^T = \left\{ \begin{array}{cccccccc} \theta_F & \theta_{Tout} & \theta_{Din} & \theta_W & \dot{\theta}_F & \dot{\theta}_{Tout} & \dot{\theta}_{Din} & \dot{\theta}_W \end{array} \right\}^T \tag{10}$$

The equations of motion in state space form are obtained using the gear ratios and Eq. (3):

$$\begin{cases} F_1 = \dot{y}_1 = y_5 \\ F_2 = \dot{y}_2 = y_6 \\ F_3 = \dot{y}_3 = y_7 \\ F_4 = \dot{y}_4 = y_8 \\ F_5 = \dot{y}_5 = -\dfrac{k_C}{I_F}(y_1 - n_T y_2) \\ F_6 = \dot{y}_6 = \dfrac{k_C\left(n_T y_1 - n_T^2 y_2\right) + k_D\left[y_3 - y_2 - g_1(\beta_1, y_2) + g_2(\beta_2, y_3)\right] f_{H1}(\beta_1, y_2)}{I_{Tout} + I_{Sec} n_{T2}^2 + I_{Tin} n_T^2} \\ F_7 = \dot{y}_7 = \dfrac{-k_S\left(y_3 n_D^{-2} + n_D^{-1} y_4\right) + k_D\left[y_2 - y_3 + g_1(\beta_1, y_2) - g_2(\beta_2, y_3)\right] f_{H2}(\beta_1, y_3)}{I_{Din} + I_{Dout} n_D^{-2}} \\ F_8 = \dot{y}_8 = -\dfrac{k_S}{I_W}\left(\dfrac{y_3}{n_D} + y_4\right) \end{cases} \tag{11}$$

2.1 Finding the equilibrium points

Equilibrium points were calculated making $\{\dot{y}\} = \{0\}$ in Eq. (11):

$$\begin{cases} y_5 = y_6 = y_7 = y_8 = 0 \\ y_1 = n_T y_2 \\ f_{H1}(\beta_1, y_2)\left[y_3 - y_2 - g_1(\beta_1, y_2) + g_2(\beta_2, y_3)\right] = 0 \\ f_{H2}(\beta_2, y_3)\left[y_2 - y_3 + g_1(\beta_1, y_2) - g_2(\beta_2, y_3)\right] = 0 \\ y_4 = -\dfrac{y_3}{n_D} \end{cases} \tag{12}$$

Based on the previous equations, equilibrium points can be found assuming $y_1 = n_T y_2$ and $y_4 = -y_3/n_D$ with the following restrictions:

$$\begin{cases} f_{H1}(\beta_1, y_2) = 0, \text{ and } f_{H2}(\beta_2, y_3) = 0 \\ \text{or} \\ y_2 + g_1(\beta_1, y_2) = y_3 + g_2(\beta_2, y_3) \end{cases} \tag{13}$$

The first equation on Eq. (13) results on the following equilibrium points:

ISSN 2176-5480

$$f_{H1}(\beta_1, y_2) = 0, \text{ and } f_{H2}(\beta_2, y_3) = 0 \rightarrow y_2 = \frac{1}{2}\arccos\left(-\frac{2}{\beta_1^2}\right), \text{ and } y_3 = \frac{1}{2}\arccos\left(-\frac{2}{\beta_2^2}\right) \tag{14}$$

To satisfy these trigonometric relationships it is necessary to assume joint angles greater than 80°, out of the commonly usage range:

$$\frac{1}{2} \leq 1 \rightarrow \beta \leq -\sqrt{2}rad, \text{ or } \beta \geq \sqrt{2}rad \rightarrow \beta \leq -81.02°, \text{ or } \beta \geq 81.02° \tag{15}$$

With the second condition of Eq. (13), equilibrium points are obtained imposing the shaft angles β_1, β_2 and an angular displacement as input.

$$y_2 + 2\left(\frac{\beta_1^2}{4}\right)\cos(2y_2) = y_3 + 2\left(\frac{\beta_2^2}{4}\right)\cos(2y_3) \tag{16}$$

Tiba (2006) affirms that Eq. (4) is valid for $\beta \leq 30°$. Figures 5(a) to 5(c) were obtained imposing the angle transmission equilibrium position θ_{Tout} in the range between 0° and 360° for β_1 equal 0°, 10° and 20°. The joint angle β_2 was varied from 0 to 20°. The equilibrium position θ_{Din} of the differential was calculated from Eq. (16) using the MATLAB® function fsolve. Figure 5(a) shows that, for $\beta_1 = 0°$, the difference between equilibrium points $\theta_{Din} - \theta_{Tout}$ was found nearby zero on the surroundings of $\beta_2 = 0°$, increasing up to 2° when $\beta_2 = 20°$. Figure 5(b) and 5(c) presented a reduction on the angle difference in equilibrium only on the surroundings of $\beta_1 = \beta_2$. It is possible to notice that the equilibrium point difference varied in amplitude depending on the value chosen for θ_{Tout}. In all next results, were the x axis displays only θ_{Tout}, it will mean that the whole complete set of equilibrium states ($\{y_{eq}\}$) was applied to the system.

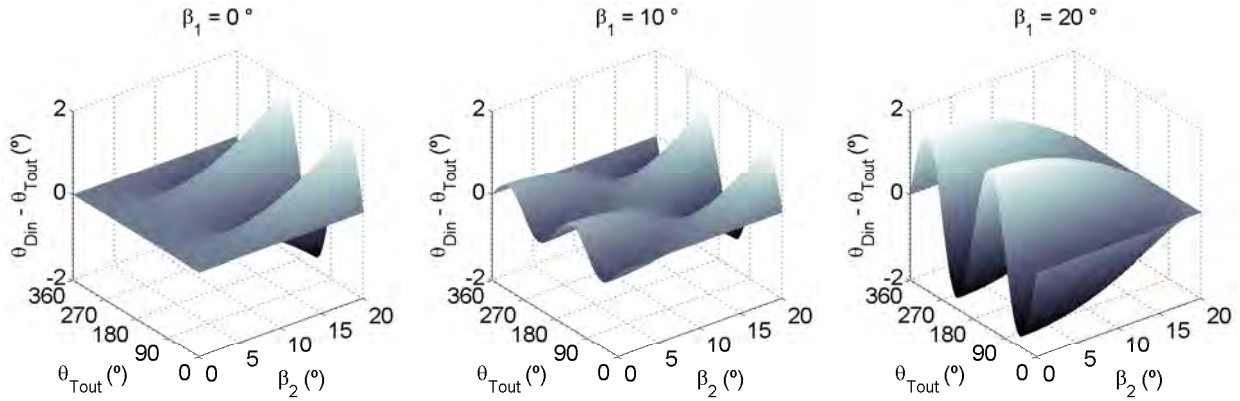

(a) (b) (c)

Figure 5. Equilibrium points found forβ_1 = 0, 5 and 10 degrees shown in (a), (b) and (c).

3. MODAL PROPERTIES OF THE LINEAR EQUIVALENT SYSTEM

The linear representation following the coordinates shown is Fig. 4(b) provides the equations of motion of Eq. (11) with mass and stiffness matrices shown in Eq. (18) and (19):

$$[M]\left\{\ddot{\theta}\right\} + [K]\{\theta\} = \{0\}, \text{ with } \{\theta\} = \left\{\begin{array}{cccc}\theta_F & \theta_{Tout} & \theta_{Din} & \theta_W\end{array}\right\}^T \tag{17}$$

$$[M] = \begin{bmatrix} I_F & 0 & 0 & 0 \\ 0 & I_{Tin}n_T^2 + I_{Sec}n_{T2}^2 + I_{Tout} & 0 & 0 \\ 0 & 0 & I_{Din} + I_{Dout}n_D^{-1} & 0 \\ 0 & 0 & 0 & I_W \end{bmatrix} \tag{18}$$

$$[K] = \begin{bmatrix} k_c & -k_c n_T & 0 & 0 \\ -k_c n_T & k_c n_T^2 + k_d & -k_d & 0 \\ 0 & -k_d & k_d + k_s n_D^{-2} & k_s n_D^{-1} \\ 0 & 0 & k_s n_D^{-1} & k_s \end{bmatrix} \tag{19}$$

ISSN 2176-5480

The first mode (Fig. 6(a)) represents the rigid body mode, not relevant for this study. The shuffle phenomenon occurs with an amplitude configuration shown by Fig. 6(b), where the vehicle moves with important levels of vibration if compared to the rest of the powertrain, and even looking to other mode configurations. Figure 6(c) displays the rattle mode configuration where the transmission and differential have the greatest amplitudes of vibration, while the flywheel and wheels remain with no significant levels of vibration. Finally, high levels of vibration occur in the differential in the fourth mode (Fig. 6(d)) where flywheel and differential moves in opposition of phase. This condition is the only that produces a real increase of effort on the driveshaft, once that, in all other cases, transmission and differential presented practically similar levels of vibration in an in-phase movement.

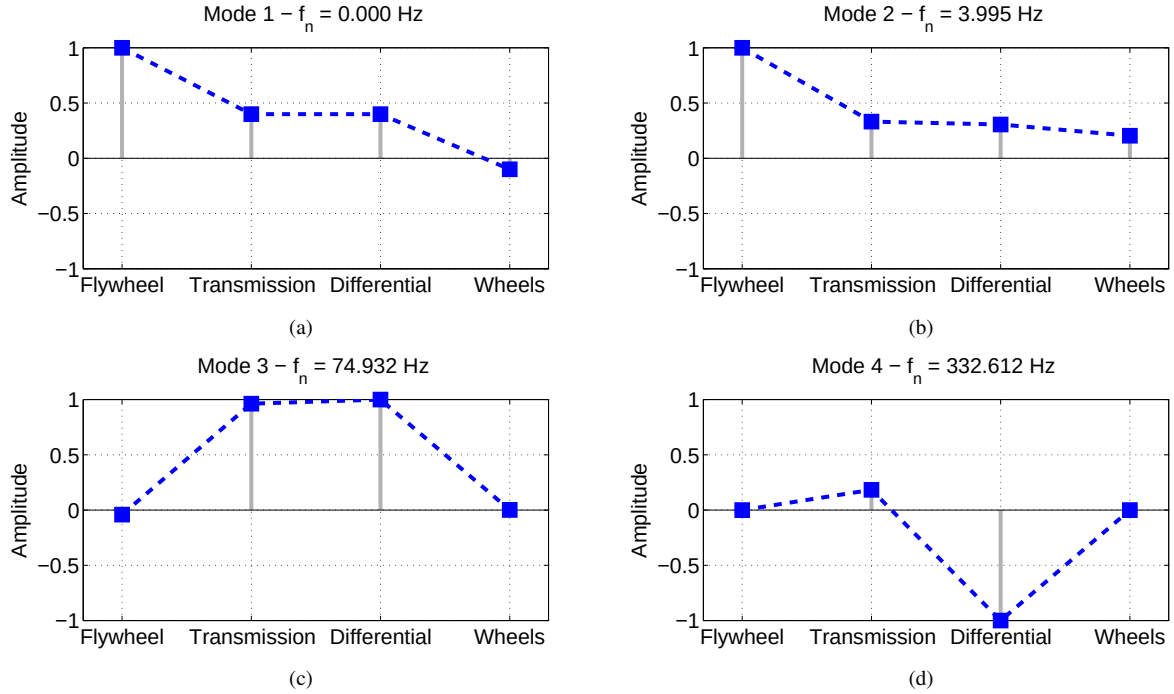

Figure 6. Modes 1, 2, 3 and 4 of linear model of Fig. 3b.

4. LINEARIZATIONS ON EQUILIBRIUM POINTS AND THE ORGANIZATION OF EIGENPROPERTIES

The nonlinear equations of system (Eq. (11)) were linearized around equilibrium points (Meirovitch, 1975). To this purpose the Jacobian was calculated (Eq. (20)) and the eigenvalues of the system were obtained from the linearized system evaluated on equilibrium states ($\{y_{eq}\}$):

$$[J] = \left[\begin{array}{ccc} \frac{\partial F_1}{\partial y_1} & \cdots & \frac{\partial F_1}{\partial y_8} \\ \vdots & \ddots & \vdots \\ \frac{\partial F_8}{\partial y_1} & \cdots & \frac{\partial F_8}{\partial y_8} \end{array}\right]\Bigg|_{\{y\}=\{y_{eq}\}} \tag{20}$$

The right and left eigenvectors ($\{\psi_R\}_i$ and $\{\psi_L\}_i$) were obtained from Eq. (21) and (22), respectively (Meirovitch, 1980):

$$[J]\{\psi_R\}_i = \lambda_i \{\psi_R\}_i \tag{21}$$

$$[J]^T \{\psi_L\}_i = \lambda_i \{\psi_L\}_i \tag{22}$$

For comparison, the linear eigenvalues were distinct (Fig. 6(a) to 6(d)), allowing the matrix containing the left eigenvectors ($[\Phi_L]$) to be obtained from the inverse of the one containing right eigenvectors ($[\Phi_R]$) (Meirovitch, 1980):

$$[\Phi_L]^T = [\Phi_R]^{-1} \tag{23}$$

ISSN 2176-5480

To compare the Jacobian eigenvalues with the linear characteristics found in Fig. 4(b), the Modal Assurance Criterion (MAC) (Allemang, 2003) was applied between the linear model left and right eigenvectors ($\{\phi_R\}$ and $\{\phi_L\}$) and the results of Eq. (21) and (22). Jacobian eigenvalues were ordered in terms of module and signal. An important point is that Eq. (21) and Eq. (22) gives eigenvalue pairs for each vibration mode. Once ordered, for example, eigenvectors 1 and 2 from the Jacobian could be compared to the first vibration mode of the linear representation. Equation 24 makes a comparison for the right eigenvectors. Due to the state space adopted in Eq. (10), only the upper part of the Jacobian eigenvector was used for right eigenvectors ($\{\psi_R\}_{N/2\times 1}$) and the first columns for left ones ($\{\psi_L\}_{1\times N/2}$).

$$MAC_R = \frac{|\{\phi_R\}^H \{\psi_R\}_{N/2\times 1}|^2}{\{\phi_R\}\{\phi_R\}^H \{\psi_R\}^H_{N/2\times 1}\{\psi_R\}_{N/2\times 1}} \tag{24}$$

$$MAC_L = \frac{|\{\phi_L\}^H \{\psi_L\}_{1\times N/2}|^2}{\{\phi_L\}\{\phi_L\}^H \{\psi_L\}^H_{1\times N/2}\{\psi_L\}_{1\times N/2}} \tag{25}$$

Figures 7(a) to 7(d) show the results of Eq. (24), while Figs. 8(a) to 8(d) are calculated with Eq. (25) for $\beta_2 = 20°$. For all cases in this study, MAC_R and MAC_L was found nearby 1.

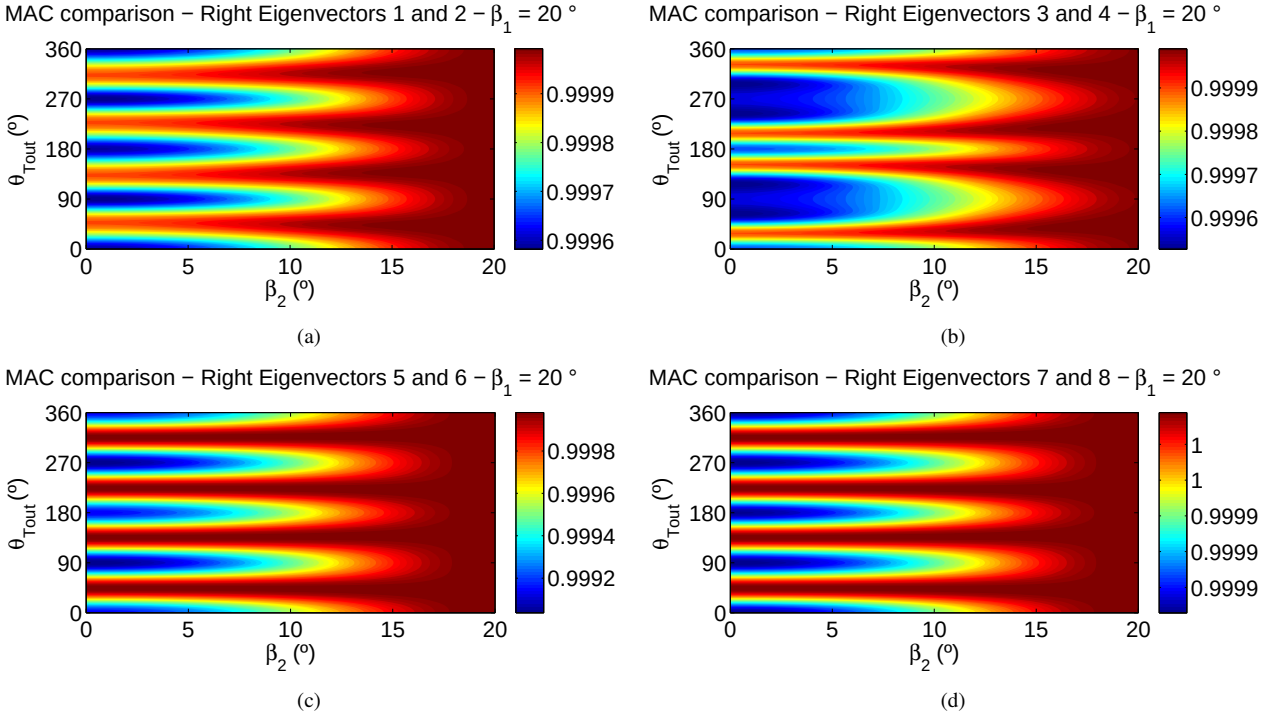

Figure 7. MAC comparison between linear and Jacobian right eigenvectors with $\beta_1 = 20°$.

4.1 Jacobian real eigenvalues at equilibrium state

The first and second eigenvalues in most of situations were purely real, equal in module but opposed in signal. The real and imaginary parts reveal that the second eigenvalue was positive real in most of cases, causing the equilibrium conditions to be unstable (Fig. 9(a), 9(b) and 9(c)). When $\beta_1 = 0°$ (Fig. 9(a)), an increased value of β_2 resulted in augmentation of its magnitude. For $\beta_1 = 10°$ (Fig. 9(b)), increase β_2 resulted in reduction of its real part up to $\beta_1 = \beta_2 = 10°$, where the real part vanishes. If $\beta_2 > 10°$ the eigenvalue becomes purely real with an increasing module. With $\beta_1 = 20°$ (Fig. 9(b)), situations where $\beta_2 < \beta_1$ resulted in reduction of the real part, that disappeared for $\beta_1 = \beta_2 = 20°$. For all cases tested, the positive real part of the eigenvalue vanished depending on the equilibrium state tested. Sets of equilibrium conditions chosen for θ_{Tout} equal 0°, 90°, 180°, 270° and 360° also presented no significant real part.

4.2 Jacobian eigenvalues with negative real part at equilibrium state

All other Jacobian eigenvalues occurred in pairs of complex conjugate imaginary numbers with no real part, presenting properties that are related to the linear model (Fig. 3b). In Fig. 10(a), 10(b) and 10(c), there are the natural frequencies

ISSN 2176-5480

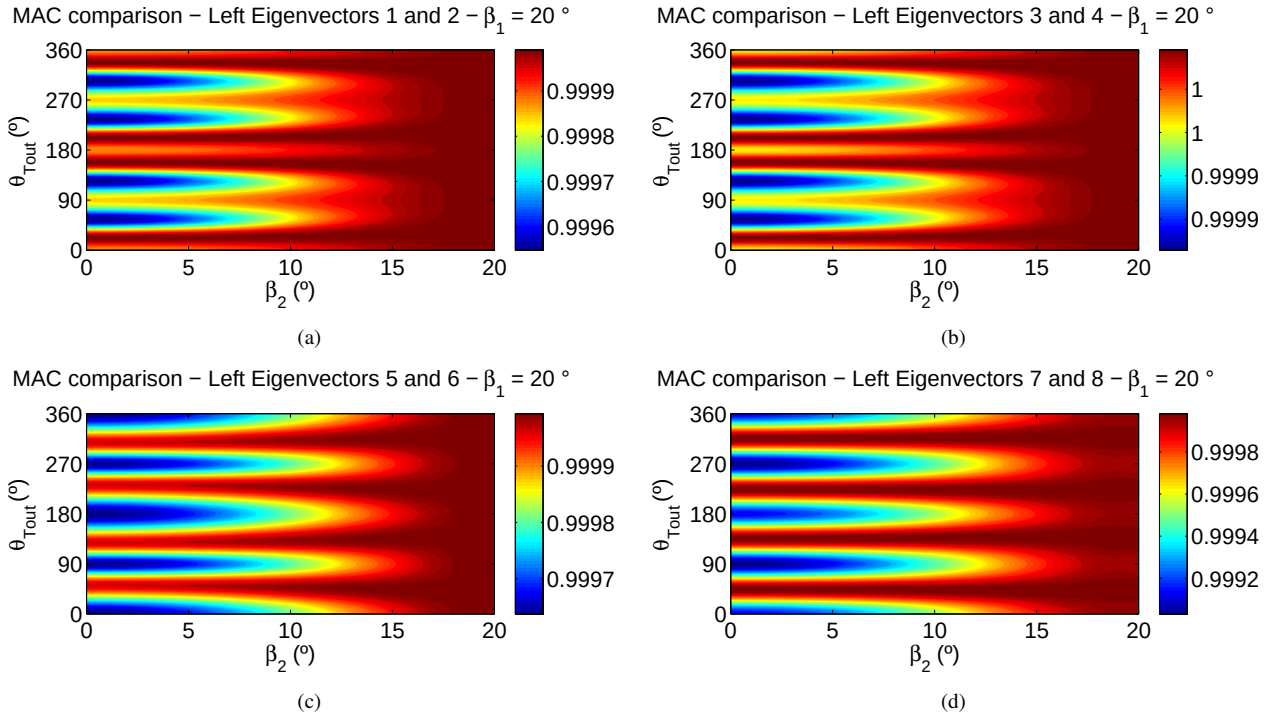

Figure 8. MAC comparison between linear and Jacobian left eigenvectors with $\beta_1 = 20°$.

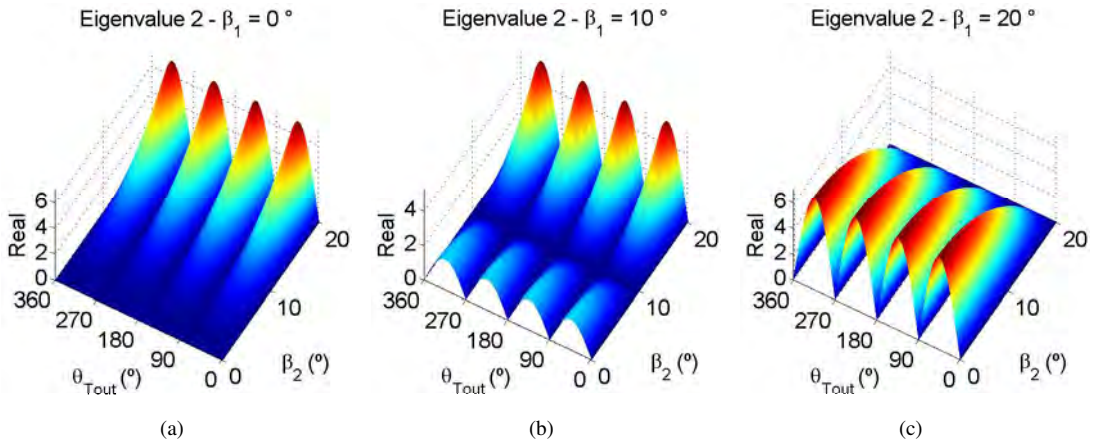

Figure 9. Real part of the second eigenvalue for β_1 adopted as 0° (a), 10° (b) and 20° (c).

found for $\beta_1 = 0°$. In all cases, for $\beta_1 = \beta_2 = 0°$ the Jacobian eigenvalues where equal to the ones found for the linear case. When the joint angles where different, all eigenvalues varied in an oscillatory manner with the equilibrium condition tested. The greater the values assumed for β_2, the greater was the peak of the natural frequency and its range of occurrence. Figures 10(a) and 10(b), related to the second and third natural frequencies of the linear model, presented variations of less than 1 Hz, while Fig. 10(c) varied in 20 Hz depending on the equilibrium for $\beta_2 = 20°$.

Reduced oscillations occur on eigenvalue pairs 3-4 and 5-6 if $\beta_1 = \beta_2 = 10°$ in Fig. 11(a) and 11(b) . Variations on the value are lower for $\beta_2 < 10°$ than for $\beta_2 > 10°$. Eigenvalues 7-8 varied gently with the equilibrium position if $\beta_1 = 0°$ and $\beta_2 = 10°$ (Fig. 11(c)). In this case, increase β_1 also augmented the eigenvalue oscillation according to the equilibrium set.

Figures 12(a), 12(b) and 12(c), show the natural frequencies found for $\beta_1 = 20°$. In cases where angles β_1 and β_2 were equal but different from zero, the second and third frequencies (Fig. 12(a) and 12(b)) were dependent on the equilibrium conditions chosen. Their range of occurrence was narrow, pretty close to the linear model. It did not happen for the fourth natural frequency, in Fig. 12(c). Its value was influenced by the equilibrium condition when $\beta_1 = \beta_2 = 20°$. Observing the fourth linear mode of Fig. 5d, the opposition of phase between the output shaft and the differential increased the driveshaft dynamic solicitation in this vibration configuration. Higher relative displacements are involved as outputs to the joints making this mode more sensitive to the joint angles chosen.

One interesting point is observed if a comparison is made between the eigenvalues with and without positive real

ISSN 2176-5480

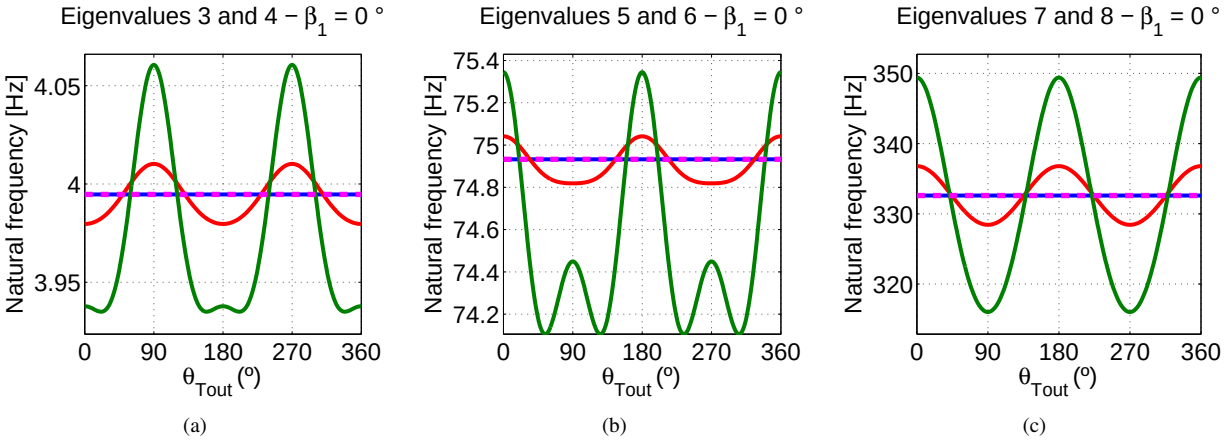

Figure 10. Natural frequencies for eigenvalues pairs 1-2 (a), 3-4 (b) and 5-6 (c), with β_1 equal to 0°. In each graphic β_2 was adopted as 0° ( ), 10° ( ), 20° ( ). Linear results ( ) are shown as reference

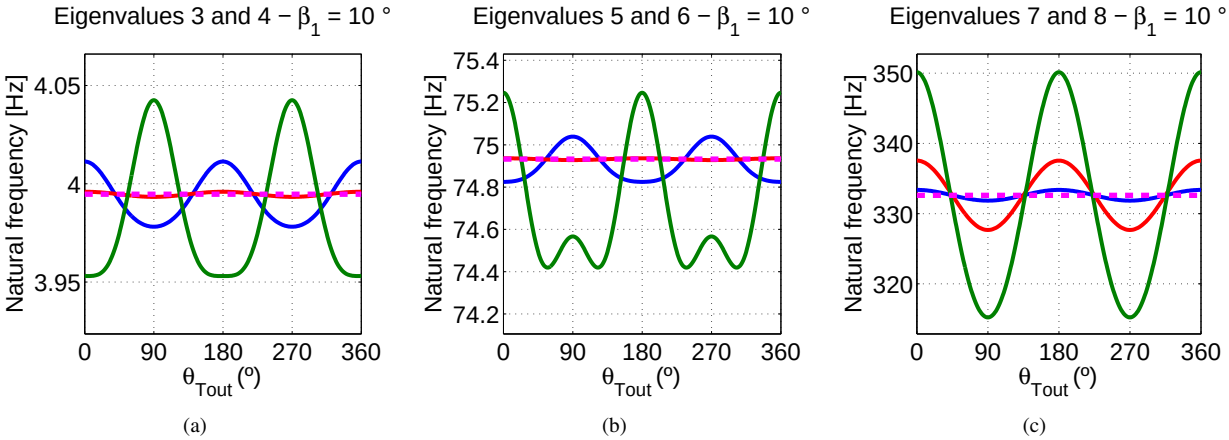

Figure 11. Natural frequencies for eigenvalues pairs 1-2 (a), 3-4 (b) and 5-6 (c), with β_1 equal to 10°. In each graphic β_2 was adopted as 0° ( ), 10° ( ), 20° ( ). Linear results ( ) are shown as reference

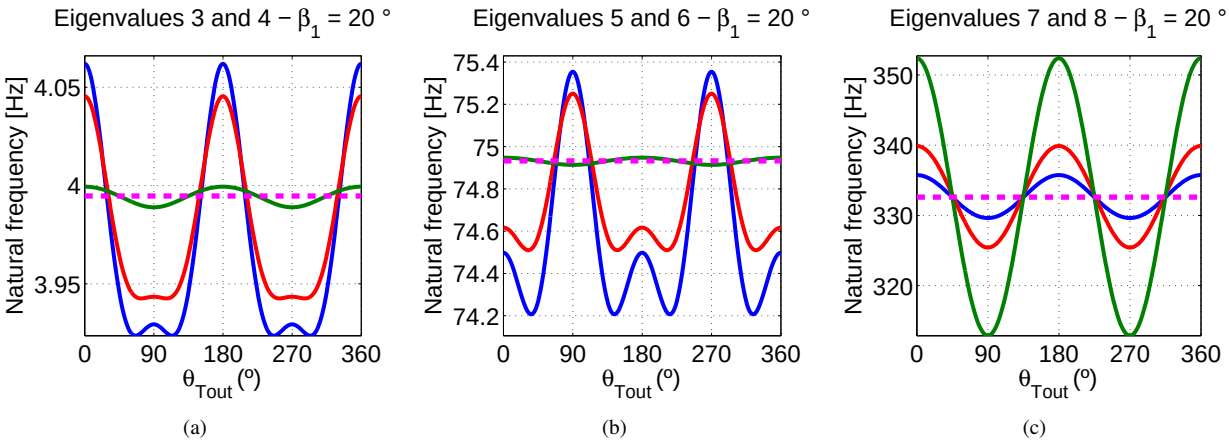

Figure 12. Natural frequencies for eigenvalues pairs 1-2 (a), 3-4 (b) and 5-6 (c), with β_1 equal to 20°. In each graphic β_2 was adopted as 0° ( ), 10° ( ), 20° ( ). Linear results ( ) are shown as reference

part. As it was explained, the real part of the lowest eigenvalues vanished for equilibrium states when θ_{Tout} was 0°, 90°, 180°, 270° and 360° (Fig. 9(a), 9(b) and 9(c)) indicating BIBO stability. If the joint angles were different, the complex conjugate eigenvalues at these conditions would have achieved great differences comparing to the linear representation as it can be seen for the third natural frequency in Fig. 10(c) and 12(c).

ISSN 2176-5480

5. CONCLUSIONS

In this work, the equilibrium conditions for the simplified powertrain model depended on the combinations of angles in the cardan joints. For the range of joint angles tested, up to 20°, the relative displacement between transmission output and differential input reached 2°, depending on the assumed position for the transmission. When the Jacobian was evaluated at equilibrium conditions, it produced eigenvalues that could be related to the linear representation, because a MAC comparison between left and right eigenvectors did not produced any significant deviations between the models. The second eigenvalue indicated unstable equilibrium conditions for almost all situations, being real positive, except for cases of equal joint angles and on specific transmission output nearby 0°, 90°, 180° and 270°. Complex conjugate eigenvalues presented natural frequencies near the ones found for the linear representation. No significant variations were obtained treating the eigenvalues related to the shuffle and rattle modes, once the vibration mode did not produce significant relative displacement on the driveshaft. The inclusion of cardan joints on these cases does not bring too much information for the designer on equilibrium states. A much more significant result was observed to the fourth mode with frequencies out of interest for torsional powertrain studies. Depending on the joint angle combinations, the fourth natural frequency presented modifications of 20 Hz.

6. ACKNOWLEDGEMENTS

The authors are thankful to CAPES and ZF Sachs do Brasil for the support.

7. REFERENCES

Albers, A., 1994. "Advanced development of dual mass flywheel (dmfw) design-noise control for today's automobiles". In *5th LuK Symposium, Bühl, Germany*.

Allemang, R.J., 2003. "The modal assurance criterion–twenty years of use and abuse". *Sound and Vibration*, Vol. 37, No. 8, pp. 14–23.

Browne, M. and Palazzolo, A., 2009. "Super harmonic nonlinear lateral vibrations of a segmented driveline incorporating a tuned damper excited by non-constant velocity joints". *Journal of Sound and Vibration*, Vol. 323, No. 1, pp. 334–351.

Couderc, P., Callenaere, J., Hagopian, J.D., Ferraris, G., Kassai, A., Borjesson, Y., Verdillon, L. and Gaimard, S., 1998. "Vehicle driveline dynamic behaviour: Experimentation and simulation". *Journal of Sound and Vibration*, Vol. 218, No. 1, pp. 133 – 157.

Crolla, D., 1978. "Torsional vibration analysis of tractor and machine pto drivelines". *Journal of Agricultural Engineering Research*, Vol. 23, No. 3, pp. 259–272.

Duditza, F., 1973. "Kardangetriebe und ihre anwendungen (cardan drive and their application)". *VDI-Verlag GmbH, Düsseldorf*.

Ligier, J.L. and Baron, E., 2002. *Acyclisme et vibrations: applications aux moteurs thermiques et aux transmissions. Notions de base*. Technip.

Meirovitch, L., 1975. *Elements of vibration analysis*. McGraw-Hill.

Meirovitch, L., 1980. *Computational methods in structural dynamics*, Vol. 5. Sijthoff & Noordhoff International Pub.

Ota, H. and Kato, M., 1984. "Lateral vibrations of a rotating shaft driven by a universal joint: 1st report, generation of even multiple vibrations by secondary moment". *Bulletin of JSME*, Vol. 27, No. 231, pp. 2002–2007.

Schmelz, F., Seherr-Thoss, H.C. and Aucktor, E., 1992. *Universal joints and driveshafts: analysis, design, applications*. Springer-Verlag New York.

Tiba, Z., 2006. "Bending and torsional vibrations of long cardan drives". *Progress in Agricultural Engineering Sciences*, Vol. 2, No. 1, pp. 1–34.

8. RESPONSIBILITY NOTICE

The authors are the only responsible for the printed material included in this paper.